CrystEngComm

Accepted Manuscript

ROYAL SOCIETY OF CHEMISTRY

www.rsc.org/crystengcomm

CrystEngComm

RSCPublishing

ARTICLE

Mannitol-assisted solvothermal synthesis of BiOCl hierarchical nanostructures and their mixed organic dyes adsorption capacities

Cite this: DOI: 10.1039/x0xx00000x

Received 00th January 2014,
Accepted 00th January 2014

DOI: 10.1039/x0xx00000x

www.rsc.org/

Fan Tian[a,§], Jinyan Xiong[a,§], Huiping Zhao[a], Yunling Liu[b], Shengqiang Xiao[c], and Rong Chen[a]*

Three-dimensional (3D) hierarchical BiOCl nanostructures constructed by interconnected two-dimensional (2D) nanoplates have been successfully synthesized *via* a facile solvothermal process with the assistance of mannitol. The products were characterized by powder X-ray diffraction (XRD), scanning electron microscopy (SEM), transmission electron microscopy (TEM) and nitrogen adsorption. In the synthesis, mannitol acted both as a capping agent and a cohesive agent to mediate the formation of hierarchical structure. A possible growth process involving crystal anisotropic growth habit and assembly process was proposed. The adsorption performance of BiOCl products for mixed organic dye removal was evaluated by using cationic rhodamine B (RhB) and anionic methyl orange (MO) as target substances. The as-prepared hierarchical BiOCl product exhibited excellent adsorption capacity and favorable recycling ability for mixed organic dyes removal. This work demonstrated a novel strategy for the design and application of well-defined complex hierarchical nanostructure.

Introduction

The worldwide increasing serious water pollution caused by synthetic dyestuffs such as rhodamine B (RhB), methyl orange (MO), congo red (CR), methylene blue (MB) and brilliant red (X-3B) has become one of considerably severe issues in environmental remediation.[1-5] With the development of nanotechnology, many current wastewater-treatment problems could be greatly ameliorated by involving nanostructured adsorbents.[5-11] Among them, three-dimensional (3D) hierarchical nanostructures have been attracted a growing attention, owing to their specific porous structures and large surface areas. To date, a variety of hierarchical nanostructures has been successfully used in adsorption, purification and separation.[6, 11-15] For example, hierarchical BiOBr nanostructures were synthesized *via* different approaches and applied as adsorbents for organic dye and heavy metal ions removal.[16-18] However, most of work focused on the single component organic dye adsorption behavior of nanostructured materials, which neglected the problems of selective adsorption and co-adsorption of mixed dyes in complicated wastewater systems. As a matter of fact, the treatment of coexisting multiple component dyes (e.g. cationic dye RhB and anionic dye MO) in wastewater still remains huge difficulties and challenges. Moreover, little attention has been paid on the desorption process of the adsorbed pollutants, which tremendously hinder the practical application. Therefore, it is significant to explore novel adsorbents with special structure and promising adsorption and desorption ability for the versatile of wastewater treatment.

Layered bismuth oxychloride (BiOCl) is one of the simplest members of the Sillén family expressed by $[M_2O_2][Cl_m]$ or $[M_3O_{4+n}][Cl_m]$ (m=1-3), where bismuth oxide based fluorite-like layers, $[M_2O_2]$ or $[M_3O_{4+n}]$, are intergrown with double chlorine layers.[19-22] The internal layered structure of BiOCl is obviously beneficial for the controllable fabrication of two-dimensional (2D) or three-dimensional (3D) nanostructures.[23-28] Up to now, although various 3D BiOCl hierarchitectures have been synthesized and their excellent photocatalytic activities have been reported, [9, 24-25, 28-33] it is still a big challenge to develop an alternative route to fabricate novel 3D BiOCl architectures with well-defined morphology and highly efficient adsorption capacity.

In this work, we successfully prepared 3D BiOCl hierarchical microstructure *via* a facile solvothermal process by involving mannitol molecules, which is an ideal morphology and structure directing agent.[28] The possible formation process of the BiOCl hierarchical microstructures involved crystal anisotropic growth habit and mannitol-assisted self-assembly process was proposed. Besides, the dye adsorption capacity of the as-synthesized BiOCl hierarchical microstructures for mixed organic dyes was investigated, which has not been reported previously. This work not only provides a new strategy

to fabricate BiOCl hierarchical microstructure, but also benefits to better understanding the mixed dye adsorption behavior and the correlation between structure and adsorption property of nanomaterials, which could direct the design and practical application of nanostructured absorbents.

Experimental

Chemical

Bismuth nitrate pentahydrate ($Bi(NO_3)_3{\cdot}5H_2O$), sodium chloride (NaCl), mannitol, ethylene glycol (EG), diethylene glycol (DEG) were purchased from Sinopharm Chemical Reagent Co., Ltd. (Shanghai, China). RhB and MO were purchased from Aladdin (Shanghai, China). All the reagents were analytical grade and used directly without further purification.

Synthesis

In a typical synthesis, 0.486 g $Bi(NO_3)_3{\cdot}5H_2O$ (1mmol) was put into a 50 mL round-bottom flask which contained 0.182 g mannitol (1 mmol) and 25 mL ethylene glycol (EG). The mixture was stirred and sonicated until $Bi(NO_3)_3{\cdot}5H_2O$ was dissolved, followed by addition of 5 mL saturated sodium chlorate solution, resulting in a transparent solution. Then the mixture was transferred to a Teflon-lined stainless steel autoclave to perform solvothermal process at 150 ºC for 12 hours. After cooling down to room temperature naturally, the solid product was collected by centrifugation and washed with deionized water for five times to remove remaining impurity. The sample was finally dried in a desiccator for a few days at room temperature for further characterization (**S1**). Other BiOCl samples (**S2~S10**) were also prepared under identical conditions by varying the experimental parameters, including solvent, reaction time and the amount of mannitol, which are listed in Table 1.

Table 1 Experimental conditions for the synthesis of BiOCl nanostructures[a]

Samples	Solvent	Mannitol (mmol)	Reaction time (h)
S1	EG	1	12
S2	EG	0	12
S3	EG	0.4	12
S4	EG	5	12
S5	EG	0.4	3
S6	EG	0.4	6
S7	DEG	0	12
S8	DEG	0.4	12
S9	DEG	1	12
S10	DEG	5	12

[a] The amount of $Bi(NO_3)_3$ is 1 mmol, and the volume of saturated NaCl solution is 5 mL. The volume of the solvent is 25 mL. The reaction temperature is 150 ºC.

Characterization

Powder X-ray diffraction (XRD) was carried on Bruker axs D8 Discover (Cu Kα = 1.5406 Å). The scanning rate is 1° min^{-1} in the 2θ range from 10 to 80 degree. Scanning electron microscopy (SEM) images were taken on a Hitachi S4800 scanning electron microscope operating at 5 eV. Transmission electron microscopy (TEM) images were recorded on a Philips Tecnai G2 20 electron microscope, using an accelerating voltage of 200 kV. Brunauer–Emmett–Teller (BET) specific surface area was analyzed by nitrogen adsorption in a Micromeritics ASAP 2020 nitrogen adsorption apparatus (USA). All the as-prepared samples were degassed at 150 ºC for 4 h prior to nitrogen adsorption measurements.

Evaluation of adsorption capacity for mixed organic dye

In the dye adsorption experiment, 0.05 g as-prepared BiOCl sample was added to 100 mL mixed dye solution (50 mL of 10 mg/L RhB and 50 mL 10 mg/L MO) with magnetic stirring in dark. At each given time interval, 2 mL suspension was sampled and centrifuged to remove BiOCl powder. Then the concentration of remained dyes was determined by the maximum absorbance (554 nm for RhB and 464 nm for MO) using a Shimadzu UV2800 UV-vis spectrophotometer. For the pH-dependent adsorption test, the pH value of mixed solution was adjusted to 3, 5, 7, 9 and 11 respectively by using 1M HCl or NaOH before adsorption. Adsorption cycle experiments were performed under pH value of 3. Desorption process was performed in an alkali solution (pH value is 11) with continuous stirring for 30 minutes in dark. All the measurements were carried out at room temperature.

Results and discussion

Morphology and structure

The composition and phase purity of the as-synthesized products were identified by powder XRD analysis. Fig. 1a shows the XRD pattern of the product prepared by solvothermal method in the presence of 1 mmol mannitol in EG (**S1**). All the diffraction peaks of as-synthesized products could be perfectly indexed to the tetragonal phase of BiOCl (JCPDS No. 73-2060). No other diffraction peak was detected, indicative of the high purity of BiOCl. The intense and sharp diffraction peaks suggest that the as-synthesized BiOCl product is well-crystallized. Moreover, the diffraction intensity ratio of (110) and (001) planes ($I_{(110)}/I_{(001)}$) is calculated to be 4.86, which is much higher than that of standard pattern (0.87 for JCPDS No. 73-2060), indicating the superior growth direction along [110] crystal orientation. The morphology and structure of the obtained BiOCl product (**S1**) were characterized by SEM images. As shown in Fig. 1b and 1c, a large quantity of 3D BiOCl hierarchical microstructure were obtained under this condition. The magnified SEM image (Fig. 1c) reveals that these 3D BiOCl hierarchical microstructure are constructed by many 2D nanoplates with a thickness of about 35 nm, which tends to interconnect with each other, forming an open porous structure through self-assembly. Fig.1d presents TEM image of individual BiOCl hierarchical microstructures, which further confirming the hierarchical structure of BiOCl product. No

distinct contrast between the edge and the center of the hierarchical nanostructures was detected, demonstrating a close-packed structure.

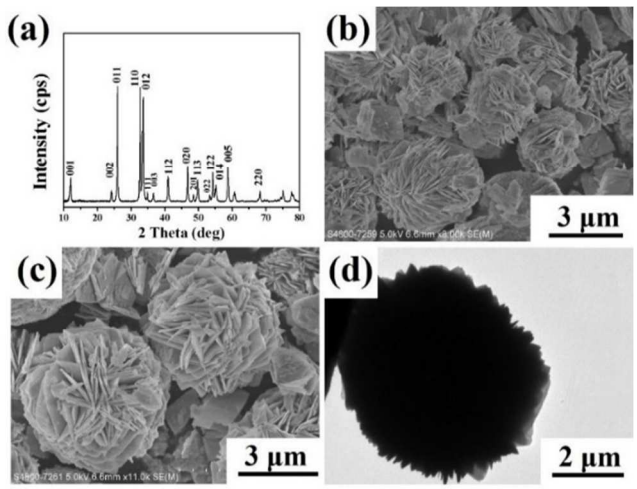

Fig. 1 XRD pattern (a), SEM (b, c) and TEM (d) images of the as-prepared BiOCl products prepared by solvothermal method in the presence of 1 mmol of mannitol in EG (**S1**).

Function of mannitol

In this synthesis, mannitol plays a crucial role in the formation of hierarchical BiOCl nanostructure. To investigate the effect of mannitol on the morphology and structure of the BiOCl products, controlled experiments were performed by varying the amounts of mannitol under identical conditions. Fig. 2 shows the XRD patterns of the as-synthesized products prepared in the absence (**S2**) and in the presence of 0.4 mmol (**S3**) and 5 mmol (**S4**) mannitol. The diffraction peaks of all the samples could be perfectly indexed to the standard pattern (JCPDS No. 73-2060), and no impurity peak was detected, indicative of the production of pure BiOCl. Noticeably, the intensity of (001) diffraction peak steadily decreases with the increase of the amount of mannitol, demonstrating that more mannitol molecules restrict the growth of BiOCl crystal along [001] crystallographic direction. To precisely understand the effect of mannitol on the crystal growth of BiOCl nanocrystal, the intensity ratio of two sets of vertical planes (i.e. $I_{(110)}/I_{(001)}$ and $I_{(020)}/I_{(001)}$) were calculated, as listed in Table 2. It was clearly observed that both of the ratio of $I_{(110)}/I_{(001)}$ and $I_{(020)}/I_{(001)}$ dramatically increased as the amount of mannitol increased from 0 to 5 mmol. Considering the high terminal oxygen density in (001) facets, which have been reported previously,[34] we proposed that the exposed oxygen atoms in BiOCl (001) facets might interact with hydroxyl of mannitol molecules *via* hydrogen bond and thus restrict the growth along [001] orientation. Fig. 3 shows the corresponding SEM images of BiOCl products obtained in the presence of different amount of mannitol after 12 h solvothermal treatment in EG. Irregular bulk 2D BiOCl microsheets were obtained in the absence of mannitol (**S2**), as depicted in Fig. 3a and 3b. With the increase of mannitol amount to 0.4 mmol (**S3**), the obtained BiOCl microsheets showed an obvious tendency of interconnection with each other, thus forming hierarchical nanostructures (Fig 3c and 3d). Ideal hierarchical BiOCl nanostructures could be fabricated in in the presence of 1 mmol mannitol (**S1**), as described in Fig. 1b and 1c. When the amount of mannitol reach 5 mmol (**S4**), well-defined sphere-like 3D BiOCl hierarchical nanostructures were also obtained (Fig. 3e and 3f). Compared with the sample fabricated in the presence of 1 mmol mannitol (**S1**), it exhibited a more closed-packed structure, indicating the cohesive role of mannitol molecules. These results indicate that mannitol could not only act as a capping agent to restrict the crystal anisotropic growth along the [001] direction, but also work as a cohesive agent to prompt the assembly of 2D microplate to 3D hierarchical structure.

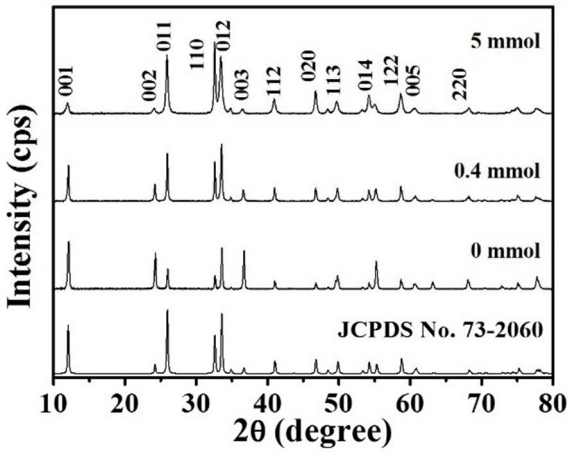

Fig. 2 XRD patterns of BiOCl products obtained after 12 h solvothermal treatment in the presence of different amount of mannitol in EG: 0 mmol (**S2**); 0.4 mmol (**S3**) and 5 mmol (**S4**).

Table 2 Diffraction intensity ratio of $I_{(110)}/I_{(001)}$ and $I_{(020)}/I_{(001)}$ of BiOCl products prepared in EG.

Samples	Mannitol (mmol)	$I_{(110)}/I_{(001)}$	$I_{(020)}/I_{(001)}$
S2	0	0.28	0.13
S3	0.4	1.11	0.36
S1	1	4.86	1.52
S4	5	6.72	2.10

The function of mannitol in the formation of hierarchical nanostructures was also investigated in DEG solvent. Controlled experiments were carried out by employing different amounts of mannitol in DEG solvent under identical experiment conditions (**S7~S10**). The obtained products were characterized by XRD and SEM, and the corresponding data were presented. Fig. 4 shows the corresponding XRD patterns of the products prepared in the presence of different amount of mannitol in DEG solvent (**S7~S10**). All diffraction patterns could also be well indexed to the tetragonal structure of BiOCl (JCPDS No. 73-2060), indicative of the production of BiOCl.

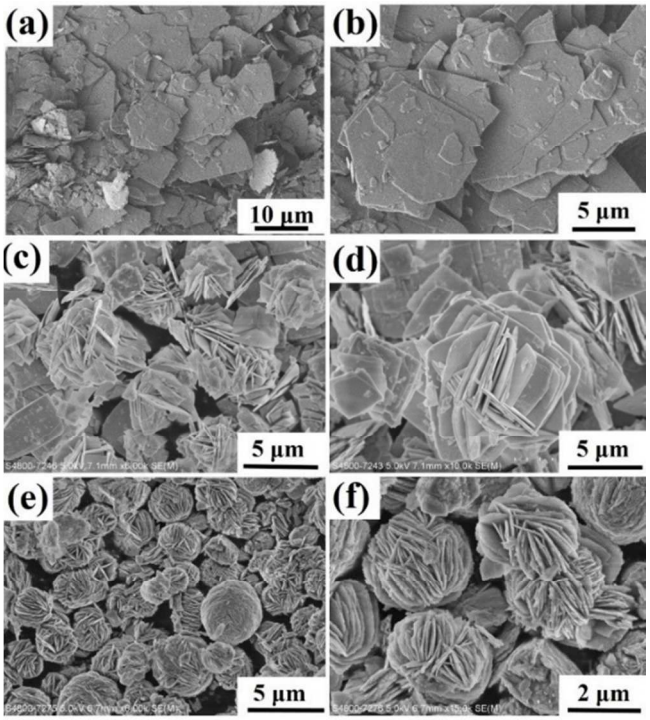

Fig. 3 SEM images of BiOCl products obtained after 12 h solvothermal treatment in the presence of different amount of mannitol in EG: 0 mmol (**S2**; a and b); 0.4 mmol (**S3**; c and d) and 5 mmol (**S4**; e and f).

Based on the obtained XRD data of different BiOCl samples, a carefully comparation of intensity ratio between (001) facet and its vertical facets were also summarized in Table 3. A similar tendency of the increase of diffraction intensity ratio ($I_{(110)}/I_{(001)}$ and $I_{(020)}/I_{(001)}$) with the increase of mannitol were also clearly observed. Fig. 5 presents typical SEM images of BiOCl products obtained in DEG. As shown in Fig. 5a and 5b, the plate-like BiOCl bulky crystals were fabricated layer by layer in the absence of mannitol. With the assistance of mannitol molecules, 2D plate-like BiOCl fragments displays an obvious tendency to fabricate hierarchical nanostructure. In the presence of 0.4 mmol mannitol, BiOCl microstructures together with 2D microplates were obtained (Fig. 5c and 5d). The increase of the amount of mannitol is beneficial for the production of 3D hierarchitectures. Fig. 5e and 5f reveal that 3D hierarchical complex structures were dominant in the product when 1 mmol of mannitol was involved. Large quantities of well-defined 3D hierarchical BiOCl nanostructures were generated in the presence of 5 mmol mannitol in DEG solvent (Fig. 5g and 5h). Noticeably, the hierarchical architectures formed in DEG solvent are slightly different with the hierarchitecture fabricated in EG solvent. It is probably due to the different physical and chemical properties of the solvents such as the viscosity, which could affect the solubility, reactivity, and diffusion behaviours of the reagents, thus directing the morphology and structure of final product. [35]

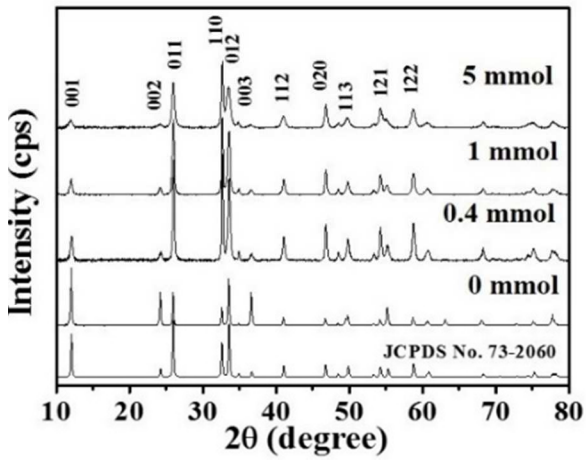

Fig. 4 XRD patterns of products synthesized in the presence of different amounts of mannitol in DEG: 0 mmol (**S7**); 0.4 mmol (**S8**); 1 mmol (**S9**) and 5 mmol (**S10**)

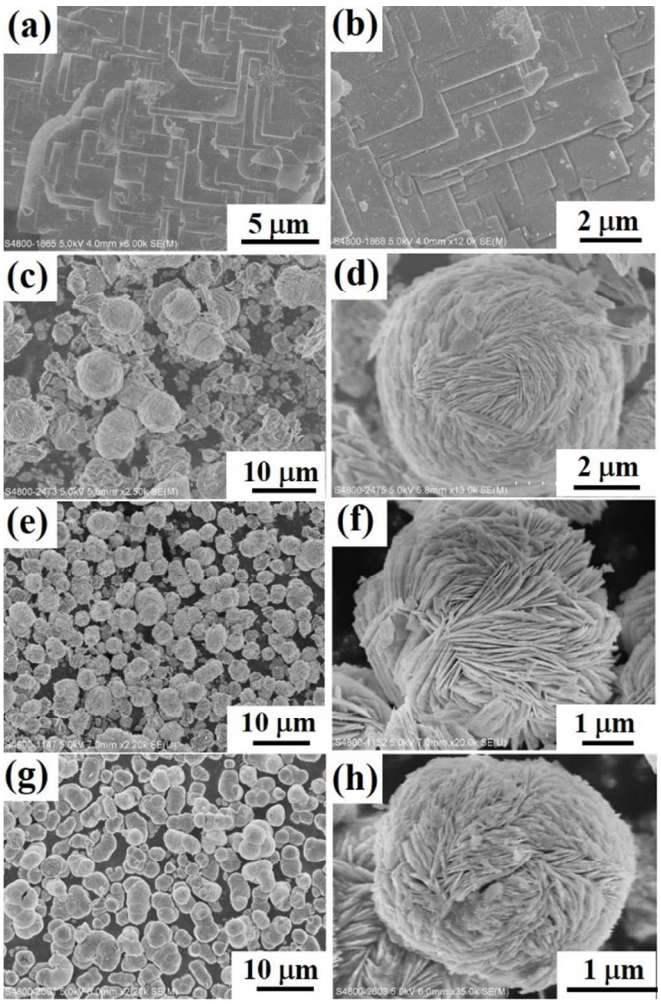

Fig. 5 SEM images of as-synthesized products in the presence of different amounts of mannitol in DEG: 0 mmol (**S7**: a, b), 0.4 mmol (**S8**: c, d), 1 mmol (**S9**: e, f), 5 mmol (**S10**: g, h), respectively.

Table 3 Diffraction intensity ratio of $I_{(110)}/I_{(001)}$ and $I_{(020)}/I_{(001)}$ of BiOCl products prepared in DEG.

Samples	Mannitol (mmol)	$I_{(110)}/I_{(001)}$	$I_{(020)}/I_{(001)}$
S2	0	0.30	0.12
S3	0.4	4.24	1.47
S1	1	4.70	1.50
S4	5	8.36	2.95

Possible formation process

To further reveal growth process of BiOCl hierarchical structures, time-dependent experiments were performed in the presence of 0.4 mmol mannitol in EG under identical condition, and the products were collected at different stages from the reaction mixture (**S5** and **S6**). Fig. 6 displays SEM images of the products obtained after 3 h (**S5**) and 6 h (**S6**) solvothermal treatment, respectively. As shown in Fig. 6a and 6b, regular square-like microplates with an obvious tendency to build up hierarchical architecture were formed after 3 h solvothermal treatment. More interestingly, the square-like microplates turned to vertically interconnect with each other. This phenomenon could be ascribed to the anisotropy of facets in BiOCl crystal under the direction of mannitol. Some high energy crystal facets may be partially covered by mannitol molecules *via* hydrogen bond interaction and thus the growth along those direction would be restricted; while the uncovered crystal facets would maintain its growth potential. A large amount of 3D BiOCl hierarchical architectures formed by microplates were fabricated after 6 h solvothermal treatment (Fig. 6c and 6d). These microplates preferred to interconnect with each other to construct a multilayered quasi-microsphere with large size, which may ascribe to the self-assemble effect of BiOCl microplates with the aid of mannitol and solvent. It is noticeable that no product was obtained after 1 h solvothermal treatment, indicating that the nucleation of BiOCl was extremely slow and no crystal growth occurred, which is probably due to the coordination between Bi^{3+} and mannitol and EG molecules, thus suppressing the hydrolysis to generate BiO^{+}.

Based on the experimental observations, a plausible formation process of the 3D BiOCl hierarchical architectures was proposed. We speculated that the formation of BiOCl 3D hierarchical structures were achieved *via* a slow nucleation, quick growth and hierarchical assembly process. As illustrated in Scheme 1, the BiOCl nuclei could be formed firstly under the solvothermal conditions. Noticeably, the nucleation process was a slow process according to our observations. When the nuclei became saturate, crystal growth took place with nucleation, and thus leading quick formation of 2D nanoplates owing to the intrinsic crystal structure of BiOCl. During the crystal growth process, mannitol molecules could selectively adsorb on the surface of the nanoplates by forming hydrogen bonds with the exposed oxygen atoms in specific facets of BiOCl to minimize the surface energy. Meanwhile, the adsorbed mannitol molecules could direct the assembly of 2D nanoplates to form intercrossed multilayered structure. Further construction of close-packed 3D hierarchical structures would occur under the synergy effect of adequate mannitol and polyol molecules. In this fabrication, mannitol not only acts as a structure-directing agent to regulate the interconnection of the nanoplates, but also further influences the arrangement of these nanoplates and leads to the formation of hierarchical assembly structures.

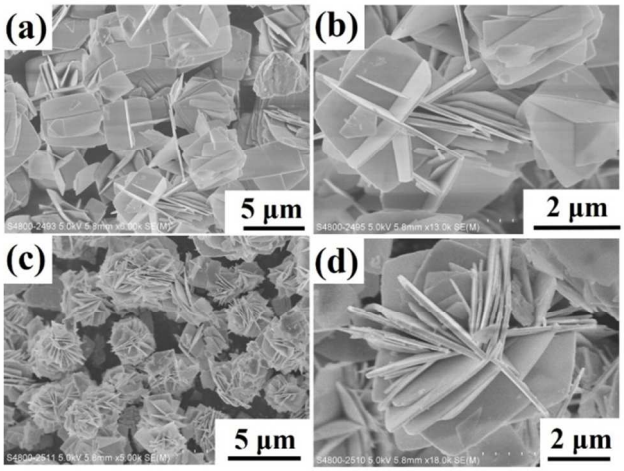

Fig. 6 SEM images of BiOCl products obtained in the presence of 0.4 mmol mannitol in EG after 3 h (**S5**: a, b) and 6 h (**S6**: c, d) solvothermal treatment.

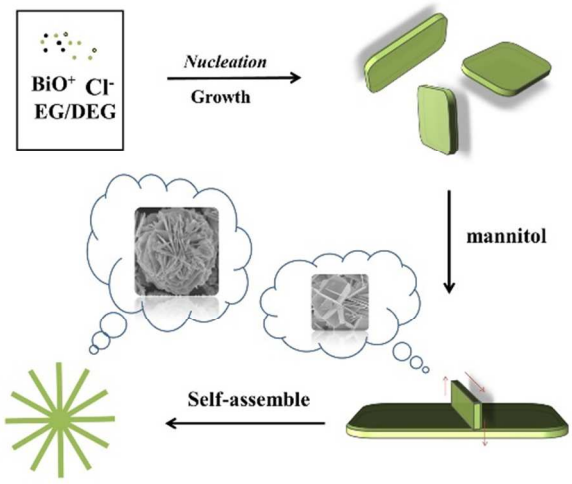

Scheme 1 Schematic illustration of the growth process of BiOCl 3D hierarchical structures.

BET surface areas

The Brunauer-Emmett-Teller (BET) specific surface areas of well-defined 3D hierarchical BiOCl nanostructures (**S4** and **S10**) and 2D BiOCl microplates (**S2** and **S7**) were investigated by nitrogen adsorption-desorption measurements. Fig. 7 displays the nitrogen adsorption-desorption isotherms of different BiOCl nanostructures. All the four isotherm profiles could be

categorized as type IV with a small hysteresis loop observed at a relative pressure of 0.4-1.0, indicating the presence of mesoporous structure in those samples. The hysteresis loops of **S2** and **S7** were relatively small, which probably due to their plates stacking structures. The BET surface areas of the different BiOCl samples calculated from the results of N_2 adsorption are 17.3, 20.4, 5.7 and 2.9 m^2/g for **S4**, **S10**, **S2** and **S7**, respectively.

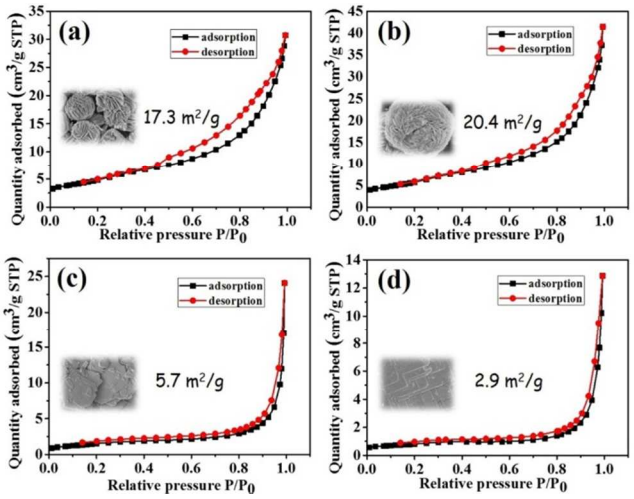

Fig.7 Nitrogen adsorption-desorption isotherms of different BiOCl samples (a) **S4**; (b) **S10**; (c) **S2** and (d) **S7**.

Dye adsorption capacity

The adsorption performance of as-prepared BiOCl samples (**S2**, **S4**, **S7** and **S10**) for mixed organic dyes removal was evaluated by using the mixture of RhB and MO as target substance. Fig. 8 shows the time-dependent RhB and MO concentration variations of the mixed dye solution over different BiOCl samples. It was clearly observed that 3D hierarchical BiOCl structure (**S4** and **S10**) displays much better adsorption abilities than that of 2D microplates (**S2** and **S7**). Among them, **S10** with largest BET surface area exhibits the best adsorption capacity, which could adsorb about 70% of RhB and 27% of MO, while **S7** with smallest BET surface area displays poor adsorption capacity for either RhB or MO. It indicates that the adsorption performance of BiOCl samples for mixed organic dye might be related to its specific structure and different BET surface areas.

To understand the adsorption behavior of BiOCl samples in the mixed dye solution, the adsorption performance of BiOCl sample for single-component organic dye (RhB and MO) was also investigated. As shown in Fig. 9a, there is a slightly decrease of adsorption capacity for RhB and increase of adsorption capacity for MO in mixed organic dye solution, indicating that the simultaneous adsorption of BiOCl for RhB and MO was a co-adsorption process. The strong interaction between cationic RhB dye and anionic MO dye was verified by three-dimensional fluorescence spectra of RhB solution and RhB/MO mixed solution. Fig. 9b and 9c present the fingerprint regions of RhB in the absence and in the presence of MO, respectively. Compared to the single component RhB solution, a clear diffusion of strong fluorescence area (the red area between emission wavelengths from 550 nm to 650 nm) was observed when MO was introduced. Meanwhile, the fluorescence intensity of area (I) (excitation: 400~450 nm; emission: 550~600) remarkably enhanced, indicating the increase of fluorescence quantum yield in the presence of MO. The obvious intensity variation of fluorescein region suggests the strong chemical interaction between RhB and MO molecules in the mixed dye solution. However, our present understanding is pretty limited, and further investigation is need in our further work.

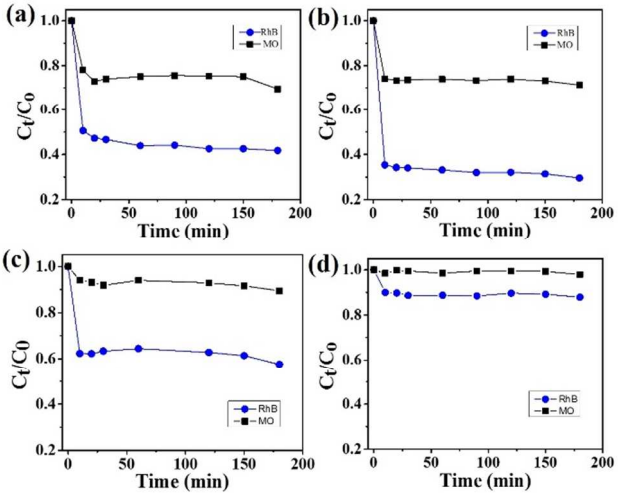

Fig. 8 Time-dependent concentration variations of RhB and MO in mixed dye solution over different BiOCl samples (a) **S4**; (b) **S10**; (c) **S2** and (d) **S7**.

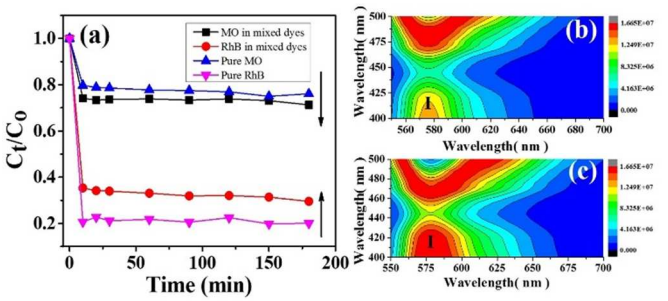

Fig. 9 Time-dependent adsorption performance of BiOCl sample (**S10**) in single-component and mixed organic dye solution (a); Three-dimensional fluorescence spectra of RhB (b) and RhB/MO mixed solution (c).

The pH effect on adsorption performance of 3D hierarchical BiOCl structures for mixed organic dye solution was also evaluated. Fig. 10a shows the mixed organic dye adsorption capacity of hierarchical BiOCl nanostructures (**S10**) under different pH values (3~11). It was found that the adsorption capacity of BiOCl sample decreased with the increase of pH value. High adsorption capacities were achieved in acidic solution, which reached 97% and 40% for RhB and MO, respectively, under the pH value of 3. While only 17% of RhB and 1% of MO was adsorbed by **S10** under the pH value 11.

From the practical application point of view, the repeatability of an absorbent is important and necessary. To evaluate the reuse ability of BiOCl samples, five cycle of adsorption-desorption experiments for RhB/MO mixed solution were conducted over hierarchical BiOCl nanostructure (**S10**). As depicted in Fig. 10b, the BiOCl product (**S10**) maintained favorable adsorption capacity after the fifth cycle run, indicating that BiOCl 3D hierarchical structures could be used as potential adsorbent in industrial application.

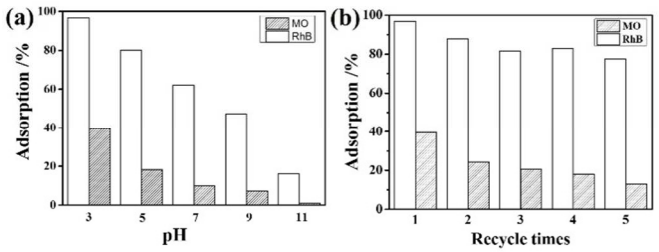

Fig. 10 Mixed organic dye adsorption capacity of BiOCl product (**S10**) under different pH values (a) and five cycle runs (b).

Conclusions

Hierarchical BiOCl structures have been successfully synthesized *via* a solvothermal process with the assistant of mannitol in polyol solvent. In this synthesis, mannitol plays a crucial role in the fabrication of 3D hierarchical nanostructures, which acts as both a capping agent and a cohesive agent to direct the assembly of BiOCl hierarchitecture. A possible growth process which involved crystal anisotropic growth habit and assembly process was also proposed. Hierarchical BiOCl nanostructures exhibit excellent adsorption capacity for mixed organic dyes removal compared with 2D plate-like BiOCl nanostructures, which was probably due to its specific structure and relatively large BET surface area. The obtained BiOCl sample also presents favorable recycling characteristics for mixed organic dye adsorption. This work not only provides a novel strategy for the design and synthesis of well-defined complex hierarchical nanostructures, but also explores significant potential adsorbent for practical wastewater treatment.

Acknowledgements

This work was supported by the National Natural Science Foundation of China (21171136), Open Research Fund of State Key Laboratory of Inorganic Synthesis and Preparative Chemistry (Jilin University, 2014-09), High-tech Industry Technology Innovation Team Training Program of Wuhan Science and Technology Bureau (2014070504020243) and Open Research Fund of State Key Laboratory of Advanced Technology for Materials Synthesis and Processing (Wuhan University of Technology, 2013-KF-6).

Notes and references

[a] School of Chemistry and Environmental Engineering, Wuhan Institute of Technology, Xiongchu Avenue, Wuhan, 430073, P.R. China.
[b] State Key Laboratory of Inorganic Synthesis and Preparative Chemistry, College of Chemistry, Jilin University, Changchun 130012, PR China
[c] State Key Laboratory of Advanced Technology for Materials Synthesis and Processing, Wuhan University of Technology, Luoshi Road, Wuhan 430070, P.R. China
§ These authors make equal contribution to this work
* Corresponding author: Prof. R. Chen, E-mail: rchenhku@hotmail.com
Tel.: (+86)13659815698; fax: (+86)2787195671.

1 R. Gong; Y. Ding; M. Li; C. Yang; H. Liu; Y. Sun, *Dyes Pigm.* 2005, ***64***, 187-192.
2 B. Cheng; Y. Le; W. Cai; J. Yu, *J. Hazard. Mater.* 2011, ***185***, 889-897.
3 R. O. Alves de Lima; A. P. Bazo; D. M. F. Salvadori; C. M. Rech; D. de Palma Oliveira; G. de Aragão Umbuzeiro, *Mutat. Res., Genet. Toxicol. Environ. Mutagen.* 2007, ***626***, 53-60.
4 M. A. Brown; S. C. De Vito, *Crit. Rev. Environ. Sci. Technol.* 1993, ***23***, 249-324.
5 J. Hu; Z. Song; L. Chen; H. Yang; J. Li; R. Richards, *J. Chem. Eng. Data* 2010, ***55***, 3742-3748.
6 J. Fei; Y. Cui; X. Yan; W. Qi; Y. Yang; K. Wang; Q. He; J. Li, *Adv. Mater.* 2008, ***20***, 452-456.
7 Y. Zhang; G. Li; H. Zhao; F. Tian; S. Xiao; R. Chen, *CrystEngComm* 2013, ***15***, 8159-8159.
8 Z. Song; L. Chen; J. Hu; R. Richards, *Nanotechnology* 2009, ***20***, 275707.
9 Y. Lei; G. Wang; S. Song; W. Fan; H. Zhang, *CrystEngComm* 2009, ***11***, 1857-1862.
10 X. Guo; G. T. Fei; H. Su; L. De Zhang, *J. Mater. Chem.* 2011, ***21***, 8618-8625.
11 Z. Dong; T. Ye; Y. Zhao; J. Yu; F. Wang; L. Zhang; X. Wang; S. Guo, *J. Mater. Chem.* 2011, ***21***, 5978-5984.
12 J. Yu; Y. Su; B. Cheng, *Adv. Funct. Mater.* 2007, ***17***, 1984-1990.
13 M. Dong; Q. Lin; H. Sun; D. Chen; T. Zhang; Q. Wu; S. Li, *Cryst. Growth Des.* 2011, ***11***, 5002-5009.
14 H. Xiao; Z. Ai; L. Zhang, *J. Phys. Chem. C* 2009, ***113***, 16625-16630.
15 T. Zhu; J. S. Chen; X. W. Lou, *J. Phys. Chem. C* 2012, ***116***, 6873-6878.
16 L. Zhang; X. F. Cao; X. T. Chen; Z. L. Xue, *J. Colloid Interface Sci.* 2011, ***354***, 630-636.
17 D. Zhang; M. Wen; B. Jiang; G. Li; J. C. Yu, *J. Hazard. Mater.* 2012, ***211–212***, 104-111.
18 G. Li; F. Qin; H. Yang; Z. Lu; H. Sun; R. Chen, *Eur. J. Inorg. Chem.* 2012, ***2012***, 2508-2513.
19 J. Geng; W.-H. Hou; Y.-N. Lv; J.-J. Zhu; H.-Y. Chen, *Inorg. Chem.* 2005, ***44***, 8503-8509.
20 X. Lin; T. Huang; F. Huang; W. Wang; J. Shi, *J. Phys. Chem. B* 2006, ***110***, 24629-24634.
21 H. Peng; C. K. Chan; S. Meister; X. F. Zhang; Y. Cui, *Chem. Mater.* 2009, ***21***, 247-252.
22 C. F. Guo; S. Cao; J. Zhang; H. Tang; S. Guo; Y. Tian; Q. Liu, *J. Am. Chem. Soc.* 2011, ***133***, 8211-8215.
23 S. Cao; C. Guo; Y. Lv; Y. Guo; Q. Liu, *Nanotechnology* 2009, ***20***, 275702.
24 J.-M. Song; C.-J. Mao; H.-L. Niu; Y.-H. Shen; S.-Y. Zhang, *CrystEngComm* 2010, ***12***, 3875.

25 L.-P. Zhu; G.-H. Liao; N.-C. Bing; L.-L. Wang; Y. Yang; H.-Y. Xie, *CrystEngComm* 2010, ***12***, 3791.
26 K.-L. Zhang; C.-M. Liu; F.-Q. Huang; C. Zheng; W.-D. Wang, *Appl. Catal., B* 2006, ***68***, 125-129.
27 Z. Deng; D. Chen; B. Peng; F. Tang, *Cryst. Growth Des.* 2008, ***8***, 2995-3003.
28 J. Xiong; G. Cheng; G. Li; F. Qin; R. Chen, *RSC Adv.* 2011, ***1***, 1542.
29 F. Chen; H. Liu; S. Bagwasi; X. Shen; J. Zhang, *J. Photochem. Photobiol., A* 2010, ***215***, 76-80.
30 J. Xiong; G. Cheng; F. Qin; R. Wang; H. Sun; R. Chen, *Chem. Eng. J.* 2013, ***220***, 228-236.
31 J. Xiong; G. Cheng; R. Wang; H. Yang; S. Xiao; R. Chen, *Sci. Adv. Mater.* 2013, ***5***, 1024-1031.
32 G. Li; F. Qin; R. Wang; S. Xiao; H. Sun; R. Chen, *J. Colloid Interface Sci.* 2013, ***409***, 43-51.
33 X. Zhang; Z. Ai; F. Jia; L. Zhang, *J. Phys. Chem. C* 2008, ***112***, 747-753.
34 J. Jiang; K. Zhao; X. Xiao; L. Zhang, *J. Am. Chem. Soc.* 2012, ***134***, 4473-4476.
35 Y. X. Zhou; H. B. Yao; Q. Zhang; J. Y. Gong; S. J. Liu; S. H. Yu, *Inorg. Chem.* 2009, ***48***, 1082-1090.

Graphical Abstract

Mannitol-assisted solvothermal synthesis of BiOCl hierarchical nanostructures and their mixed organic dyes adsorption capacities

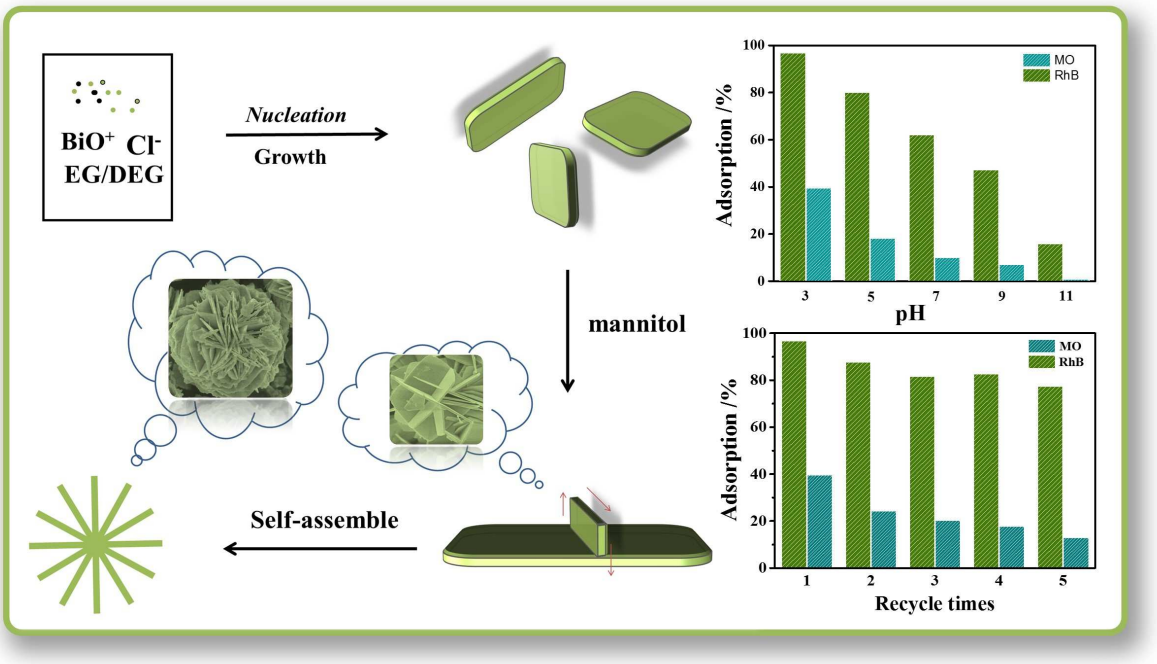

BiOCl hierarchical nanostructures constructed by interconnected nanoplates have been successfully synthesized *via* a facile solvothermal process with the assistance of mannitol, and exhibited excellent adsorption capacity and favorable recycling ability for mixed organic dyes removal.